Research Article

Xiaodong Zhu, Fengqiu Qin, Yangwen Xia, Yuanyuan Zhong, Xiuping Zhang, Wei Feng*, and Yu Jiao*

Synthesis of Ag@AgCl modified anatase/rutile/ brookite mixed phase TiO₂ and their photocatalytic property

https://doi.org/10.1515/ntrev-2022-0483 received May 22, 2022; accepted September 11, 2022

Abstract: Pure and Ag@AgCl modified TiO_2 were synthesized by one-step hydrothermal method, which exhibit anatase/rutile/brookite (A/R/B) triphasic structure. The photocatalysts were characterized by X-ray diffraction, scanning electron microscope, transmission electron microscope, X-ray photoelectron spectroscopy, photoluminescence, electrochemical impedance spectroscopy, photocurrent response, and diffuse reflectance spectroscopy, and the photocatalytic activity was evaluated by taking $100 \, \text{mL}$ ($10 \, \text{mg/L}$) methylene blue (MB) aqueous solution as the target pollutant. The results show that Ag@AgCl modification is beneficial for the separation of photogenerated charges and the absorption in visible region. The degradation degree of MB increases from 75.7% for pure TiO_2 to 97.3% for Ag@AgCl modified TiO_2 .

Keywords: TiO₂, triphasic structure, Ag@AgCl modification, photocatalytic activity

1 Introduction

As one of the new green environmental protection technologies, photocatalytic technology can be applied for the degradation of organic pollutants [1–5]. Among many photocatalytic materials, TiO₂ shows the advantages of

low cost, mild reaction conditions, high chemical stability, and no secondary pollution [6-10]. However, due to the shortcomings of TiO₂, such as low sunlight utilization and fast recombination of photogenerated charges, its photocatalytic degradation effect is greatly limited [11–13]. When noble-metals and semiconductors are combined, Schottky junctions will be formed on the interfaces, which promote the separation of photogenerated electrons and holes. On the other hand, the surface plasmon resonance (SPR) of noble-metal can enhance visible light absorption, advancing the photocatalytic performance [14-17]. Moreover, Ag@AgCl modification can further improve the photocatalytic activity on the basis of Ag modification. Wang et al. [18] prepared Ag@AgCl/TiO2 photocatalyst and found that the recombination of photoinduced electrons and holes is retarded and the absorption in visible region is enhanced through Ag@AgCl modification. Therefore, Ag@AgCl/TiO₂ shows higher photocatalytic activity than pure TiO2 and Ag/TiO₂.

It is generally believed that ${\rm TiO_2}$ with mixed crystal exhibits better photocatalytic performance than single structure owing to the mixed crystal effect. Anatase/rutile ${\rm TiO_2}$ is the focus of mixed ${\rm TiO_2}$ and has been widely studied. Basis of two-phase mixed crystal, anatase/rutile/brookite triphasic ${\rm TiO_2}$ exhibits higher photocatalytic activity than two-phase and monophase ${\rm TiO_2}$ [19–21]. It is reported by Mutuma *et al.* [22] that the photocatalytic activity of anatase/rutile/brookite three-phase mixed crystal ${\rm TiO_2}$ is higher than that of anatase/rutile two-phase mixed crystal ${\rm TiO_2}$.

In our previous work, it has been proved that the anatase/rutile/brookite triphase ${\rm TiO_2}$ shows better activity than two-phase and monophase ${\rm TiO_2}$ [20]. In the present work, the advantages of ${\rm TiO_2}$ with triphase and Ag@AgCl modification were combined to prepare Ag@AgCl modified anatase/rutile/brookite ${\rm TiO_2}$ composite by one-step hydrothermal method. The effect of Ag@AgCl modification on the structure and photocatalytic performance of anatase/rutile/brookite triphasic ${\rm TiO_2}$ were investigated.

^{*} Corresponding author: Wei Feng, School of Mechanical Engineering, Chengdu University, Chengdu, 610106, China, e-mail: fengwei233@126.com

^{*} Corresponding author: Yu Jiao, School of Science, Xichang University, Xichang 615000, China, e-mail: jiaoyu@xcc.edu.cn Xiaodong Zhu, Fengqiu Qin, Yangwen Xia, Yuanyuan Zhong, Xiuping Zhang: School of Mechanical Engineering, Chengdu University, Chengdu, 610106, China

2 Experimental

2.1 Synthesis of photocatalyst materials

Polyethylene glycol (analytical reagent, AR), butyl titanate (AR), anhydrous ethanol (AR), hydrochloric acid (AR), silver nitrate (AR), and methylene blue (MB) (AR) were purchased from Chengdu Kelong Chemical Reagent Factory (PR China).

10 mL of butyl titanate was added to 30 mL anhydrous ethanol to obtain solution A. 30 mL of deionized water, 1 mL of hydrochloric acid, and 1 mL of polyethylene glycol were mixed evenly to obtain solution B, which was added to solution A dropwise to obtain a mixture. Then, the mixture was transferred to a hydrothermal reaction kettle for hydrothermal treatment at 190°C for 15 h. The obtained powder was washed several times to neutral, and dried at 80°C in an oven. Finally, after grinding, the pure TiO₂ was prepared, which is marked as ARB.

Ag@AgCl modified TiO_2 marked as Ag@AgCl-ARB can be obtained by adding certain amount of AgNO₃ in solution B, and keeping the other steps same as the preparation procedure of ARB. The molar ratio of Ag/Ti is 2%.

2.2 Characterization

The crystal structure and phase information were studied by X-ray diffraction (XRD) using a DX-2700 X-ray diffractometer with Cu Kα radiation as the X-ray source, the scan range 2θ was $20-70^{\circ}$ and scan speed was 0.06° /s (Dandong Haoyuan Instrument Co. Ltd., Dandong, China). The morphology was observed by a JEM-F200 transmission electron microscope (TEM and HRTEM) and a Hitachi SU8220 scanning electron microscope (SEM) (FEI Company, Hillsboro, OR, USA). The composition and valence of elements were analyzed by an XSAM800 multifunctional surface analysis system (X-ray photoelectron spectroscopy, XPS) (Thermo Scientific K-Alpha, Kratos Ltd, Manchester, UK). The photoluminescence (PL) spectra were measured using an F-4600 fluorescence spectrum analyzer with an Xe lamp at an excitation wavelength of 320 nm (Shimadzu Group Company, Kyoto, Japan). The photocurrent response (PC) and electrochemical impedance spectroscopy (EIS) were measured by a DH-7000 electrochemical workstation (Beijing Jinyang Wanda Technology Co., Ltd, Beijing, China). The optical absorption was analyzed by a UV-3600

ultraviolet-visible spectrophotometer (Shimadzu Group Company, Kyoto, Japan).

2.3 Photocatalytic activity test

The photocatalytic activity of samples was evaluated by measuring the decomposition of MB. $100\,\mathrm{mL}$ of $10\,\mathrm{mg/L}$ MB aqueous solution and $0.05\,\mathrm{g}$ sample powder were mixed together and stirred in dark for $30\,\mathrm{min}$ to achieve adsorption–desorption equilibrium. Then, the irradiation was carried out using a $250\,\mathrm{W}$ Xe lamp as the light source. After centrifugal separation, the solution was taken every $15\,\mathrm{min}$ and the absorbance at $664\,\mathrm{nm}$ was measured. The degradation degree was calculated by formula $(A_0-A_t)/A_0\times 100\%$.

On the basis of the MB degradation system, $2\,\text{mL}$ (0.1 mol/L) of p-benzoquinone (BQ, $\cdot O_2^-$ trapping agent), isopropanol (IPA, $\cdot \text{OH}$ trapping agent), and ammonium oxalate (AO, h^+ trapping agent) were added to investigate the active species.

3 Results and discussion

3.1 Phase composition

Figure 1 presents the XRD patterns of samples. The diffraction peaks of ARB at 25.4, 38.0, and 48.0° are indexed

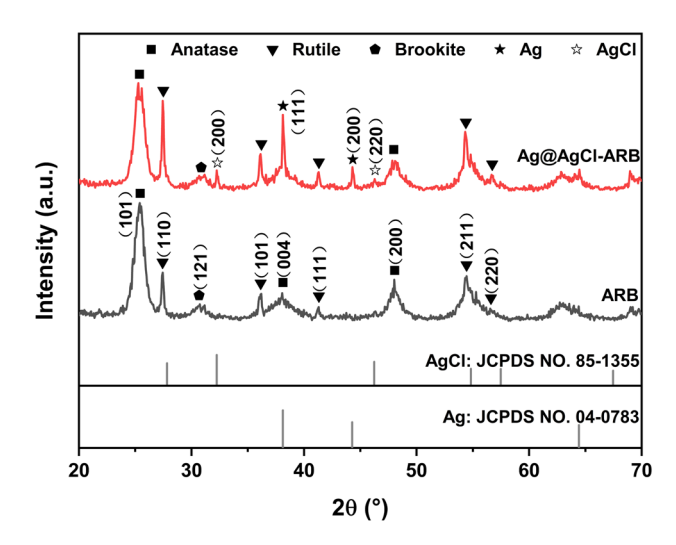


Figure 1: XRD patterns of the samples.

to the (101), (004), and (200) planes of anatase. The diffraction peaks at 27.4, 36.2, 41.3, 54.4, and 56.6° are indexed to the (110), (101), (111), (211), and (220) planes of rutile. In addition, the diffraction peak corresponding to the (121) planes of brookite appears at 31.1°, implying that the prepared ARB is composed of three phases, namely, anatase, rutile, and brookite [23]. As for Ag@AgCl-ARB, besides the anatase, rutile, and brookite phase, new diffraction peaks at 38.1 and 44.4° are indexed to the (111) and (200) planes of metallic Ag [24], and peaks at 32.3 and 46.3° correspond to the (200) and (220) planes of AgCl, respectively [19].

3.2 Morphology

Figure 2 depicts the SEM images of ARB and Ag@Ag-Cl-ARB. Both the samples are irregular in shape and ranging in size from ten to tens of nanometers. ARB and Ag@AgCl-ARB present almost the same morphology, implying that Ag@AgCl modification has no distinct influence on the morphology. Figure 2(c) and (h) are the element mappings of Ag@AgCl-ARB. The Ag@AgCl-ARB is mainly composed of Ti, O, Ag, and Cl, distributed uniformly in the sample, which demonstrates that Ag and Cl elements are present in Ag@AgCl-ARB.

Figure 3 shows TEM and HRTEM images of the samples. From Figure 3(a), it can be observed that the single particle is roughly granular, and the size is between 10-20 nm. The crystal plane spacings marked in Figure 3(c) 0.35, 0.32, and 0.29 nm can be attributed to the (101) plane of anatase, the (110) plane of rutile, and the (121) plane of brookite [20,25,26], respectively, indicating that ARB consists of anatase, rutile, and brookite phase, which is in accordance with the XRD results. Figure 3(d) shows the HRTEM images of Ag@AgCl-ARB, the crystal lattice fringes 0.35, 0.32, and 0.29 nm correspond to the crystal plane of anatase (101), rutile (110), and brookite (121), respectively.

3.3 Element composition

Figure 4(a) shows the full XPS spectra of ARB and Ag@AgCl-ARB. The Ag@AgCl-ARB is mainly composed of Ti, O, Ag, and Cl. No other impurity peaks were detected in ARB and Ag@AgCl-ARB, indicating the high purity of samples. Figure 4(b) shows the high resolution spectra of Ti 2p. Two peaks at 458.4 and 464.1 eV in the

spectrum of ARB are indexed to Ti $2p_{3/2}$ and Ti $2p_{1/2}$, verifying that the Ti element exists in 4+ valence state [27,28]. In Figure 4(c), the O 1s peaks of ARB are located at 529.6 and 530.3 eV, corresponding to lattice oxygen (O²⁻) and surface hydroxyl group (OH⁻), respectively [28]. After Ag@AgCl modification, the binding energies of Ti 2p and O 1s shift to lower position, which can be ascribed to the interaction between Ag, Cl elements, and Ti, O elements [29,30]. The peaks at Ag $3d_{5/2}$ 366.7 and Ag $3d_{3/2}$ 372.8 eV are attributed to metals Ag⁰ and Ag⁺ in Figure 4(d) [31,32]. As demonstrated in Figure 4(e), the characteristic peaks of Cl $2p_{3/2}$ and Cl $2p_{1/2}$ of Cl element are located at 197.5 and 199.0 eV, respectively, which indicate that Cl element is in -1 valence state [31].

3.4 Photogenerated charges separation analysis

Figure 5(a) shows the PL spectra of samples. Since the PL peaks are responsible for the recombination between photogenerated electrons and holes, the stronger the PL peak intensity, the higher the recombination of photogenerated charge [33]. Compared with ARB, although the PL peak positions of Ag@AgCl modified ARB does not change, the peak intensity is significantly lower than that of ARB, implying that Ag@AgCl modification retards the recombination effectively.

Figure 5(b) shows the EIS Nyquist plots of ARB and Ag@AgCl-ARB. According to Nyquist theorem, the arc radius of Ag@AgCl-ARB is smaller than ARB, which indicates that Ag@AgCl-ARB possesses lower charge movement resistance [34–36]. Figure 5(c) shows the PC curves of samples. Generally, the higher the photocurrent, the stronger the photoinduced electrons and holes separation ability [35,37]. Both ARB and Ag@AgCl-ARB produce photocurrent under light irradiation. Nevertheless, Ag@AgCl-ARB shows higher photocurrent density, implying that Ag@AgCl modification is beneficial to the separation of photoinduced charges. The electrochemical test results are consistent with PL spectra.

3.5 Optical absorption analysis

Figure 6 presents the UV-visible absorption spectra and band gap of the samples. It can be found in Figure 6(a) that the absorption edges of ARB and Ag@AgCl-ARB are basically the same, both showing absorption edges at

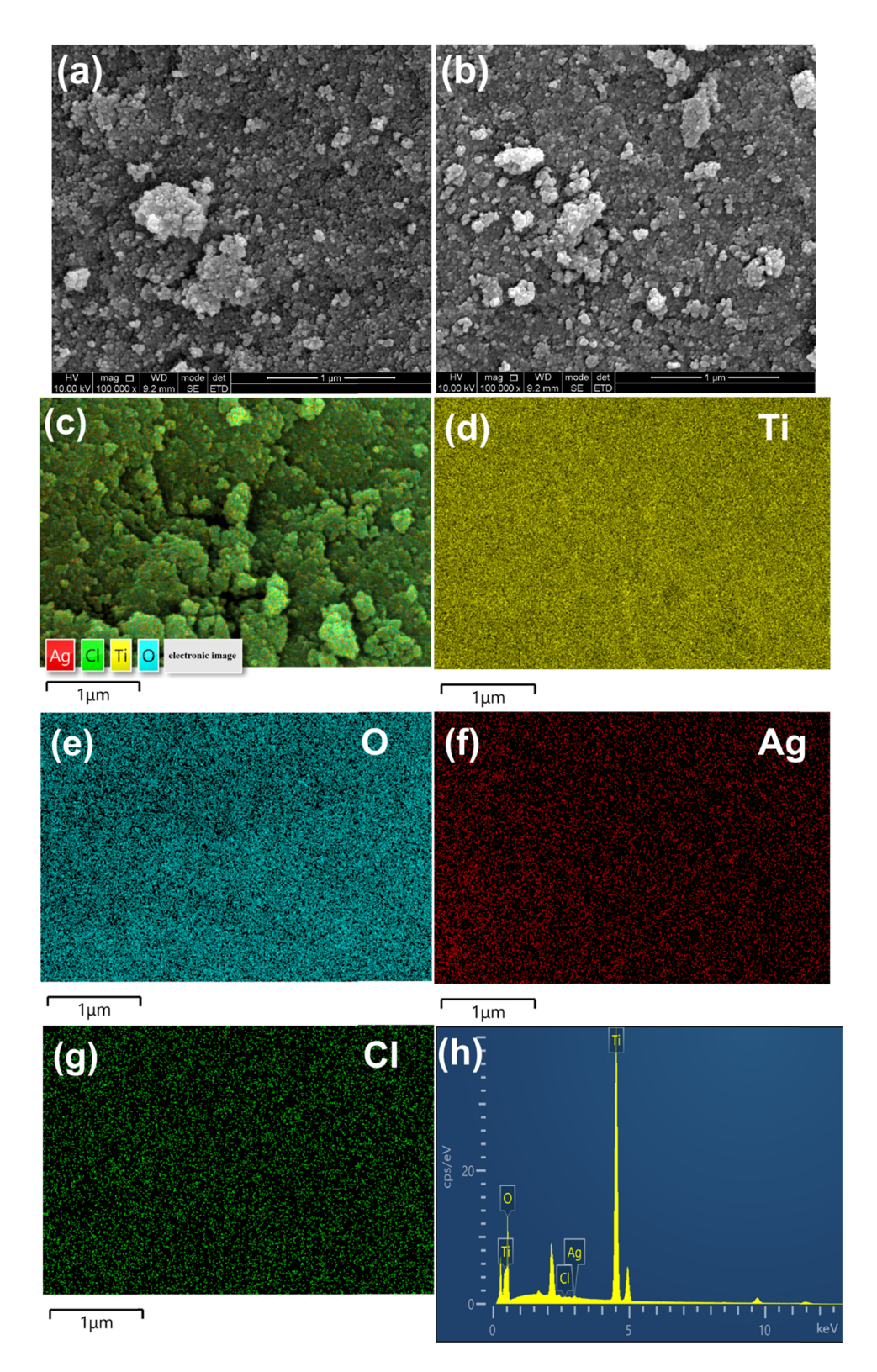


Figure 2: SEM images of ARB (a), Ag@AgCl-ARB (b), element mappings (c-g), and EDS analysis of Ag@AgCl-ARB (h).

400 nm approximately. Figure 6(b) shows the $(\alpha hv)^{1/2}$ -hv curves of the samples. The band gap width of the semiconductor can be estimated by Tauc-plot [38–40]. The

gap width of Ag@AgCl-ARB (2.84 eV) is smaller than that of ARB (2.93 eV). In the visible region, Ag@AgCl-ARB shows higher absorption than that of ARB, indicating

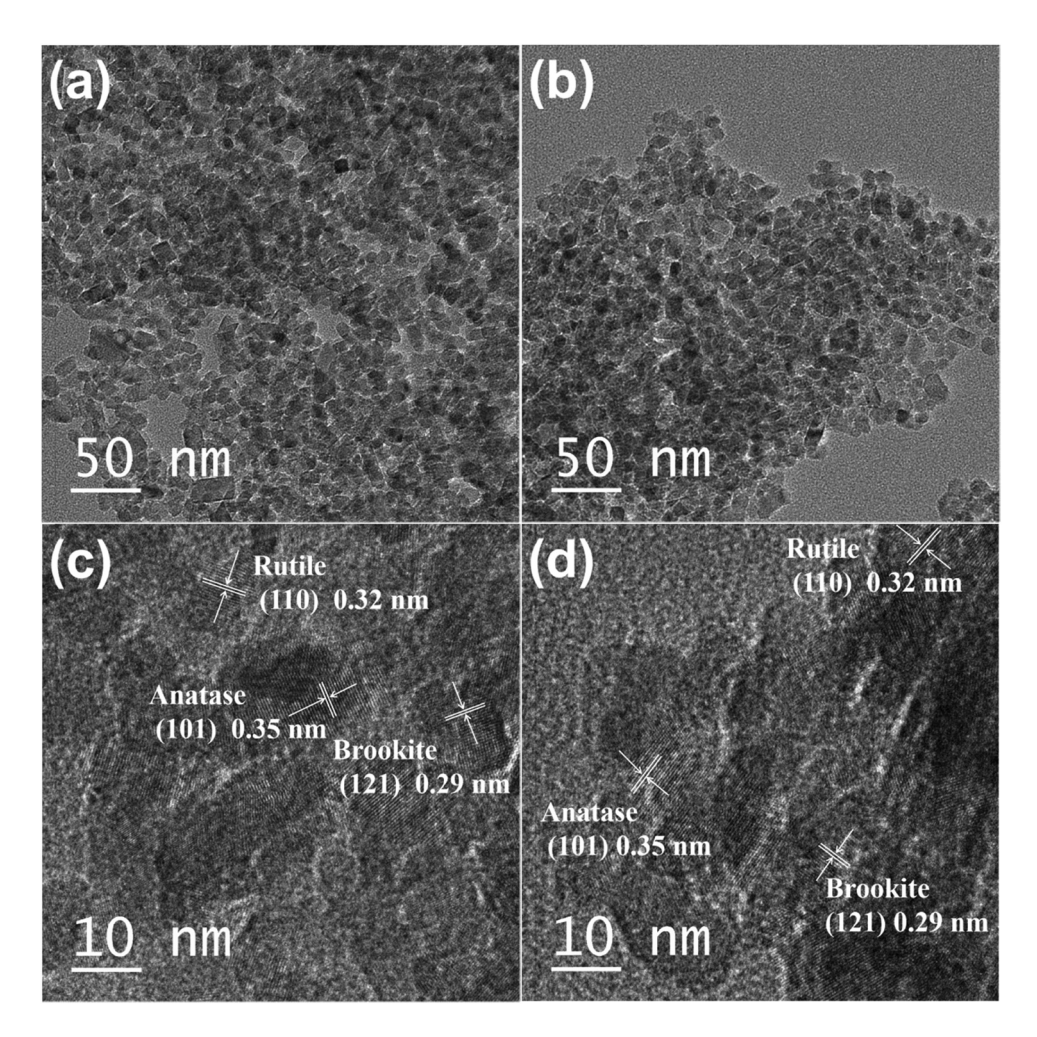


Figure 3: TEM images of ARB (a), Ag@AgCl-ARB (b), HRTEM images of ARB (c), and Ag@AgCl-ARB (d).

that the plasma resonance effect caused by Ag particles is beneficial to increasing the absorption of visible light [41].

3.6 Photocatalytic activity

Figure 7(a) presents the degradation degree curves of MB. The self-degradation of MB without photocatalyst is 8%, which is relatively low in the degradation process. Therefore, the degradation of MB is mainly derived from the presence of photocatalysts under irradiation. After illumination for 60 min, the degradation degree of MB by ARB is 75.7%, and it is 97.3% for Ag@AgCl-ARB, indicating that the photocatalytic efficiency is significantly improved for Ag@AgCl modification. For comparison, Ag-ARB (Ag/Ti = 2%) was prepared, which shows a degradation degree of 86.5%. It is proved that Ag

modification improves the photocatalytic activity of TiO₂, but the effect is inferior to Ag@AgCl modification.

The kinetics fitting results are shown in Figure 7(b). It can be found that the time t shows a linear relationship with $-\ln(C/C_0)$, which suggests that the reaction of photocatalytic degradation of MB conforms to the first-order reaction [42]. The higher the reaction rate constant, the higher the photocatalytic activity. The first-order reaction rate constants of ARB, Ag–ARB, and Ag@AgCl–ARB are 0.022, 0.032, and 0.055 min⁻¹, respectively. Ag@AgCl–ARB shows the highest k value, which is in line with the photocatalytic degradation results.

To study the reusability of Ag@AgCl-ARB photocatalyst, the cycling experiment of degradation MB was carried out. The experimental results are shown in Figure 8. As the number of cycles increases, the degradation degree of MB decreases slightly. After 5 cycles, the degradation degree of Ag@AgCl-ARB composite decreases from 97.3 to 85.2%.

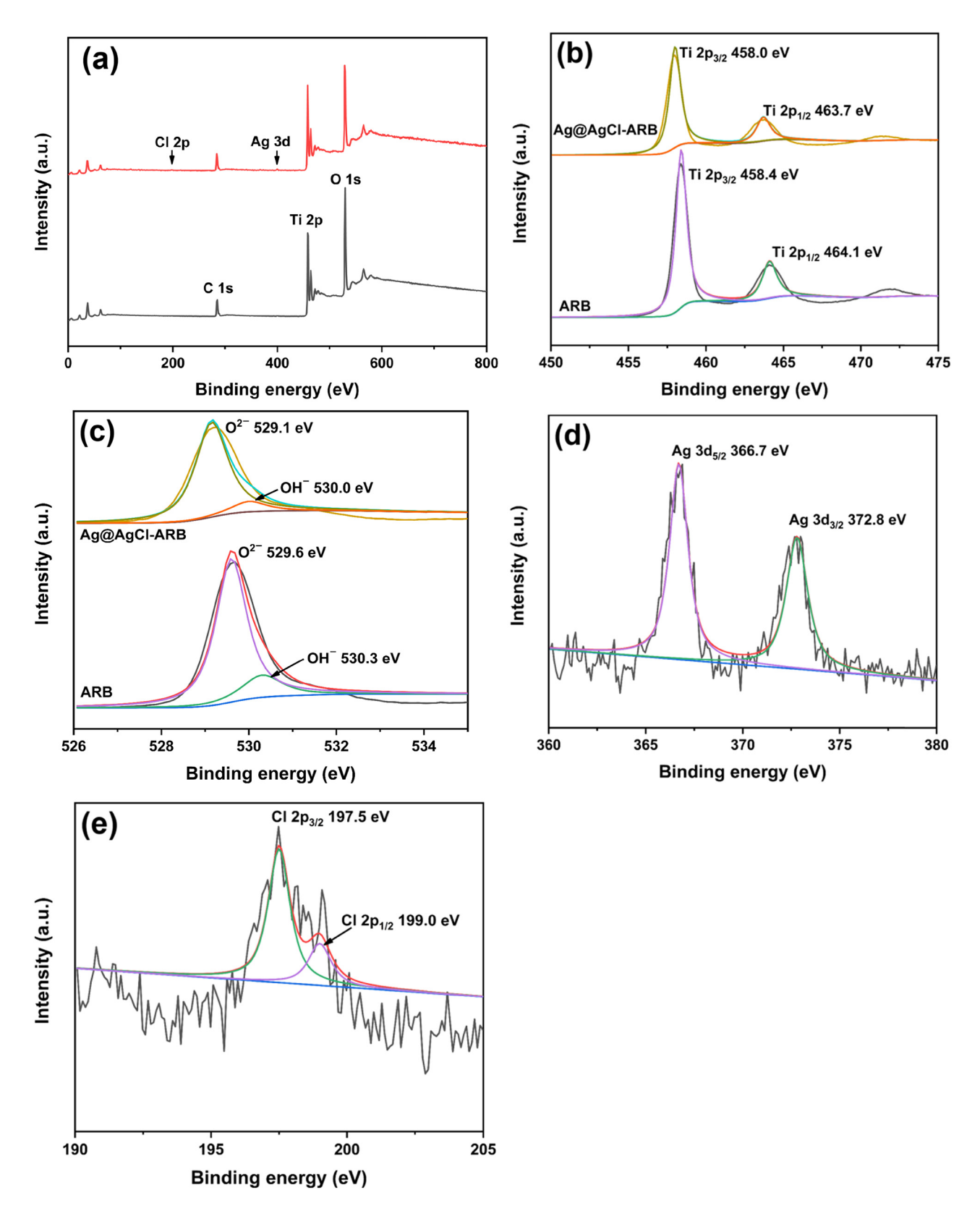


Figure 4: XPS survey of ARB and Ag@AgCl-ARB (a), high resolution spectra of Ti 2p (b), O 1s (c), Ag 3d (d), and Cl 2p (e).

2922 — Xiaodong Zhu et al. DE GRUYTER

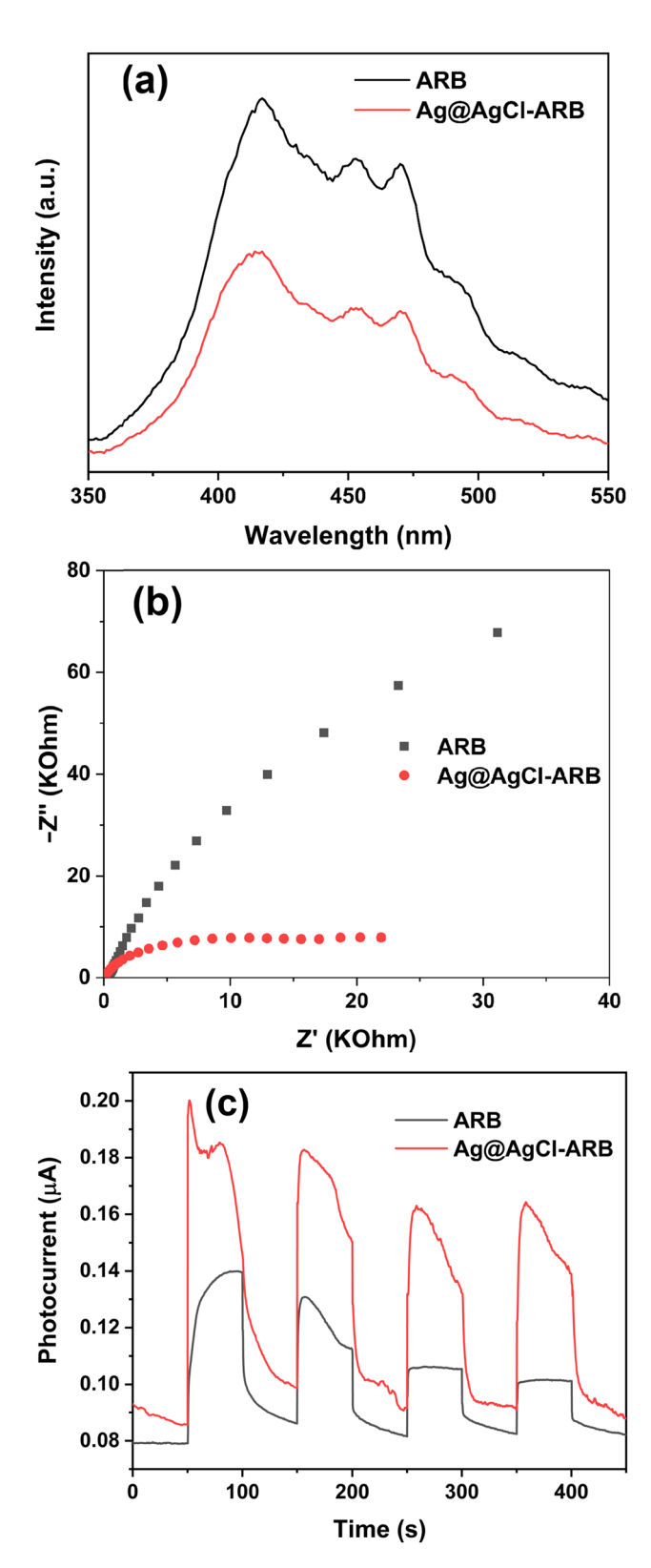


Figure 5: PL spectra (a), EIS (b), and PC curves (c) of ARB and Ag@AgCl-ARB.

The XRD pattern of Ag@AgCl-ARB composite photocatalyst after five cycles is shown in Figure 9. Compared with the initial sample, it is found that the diffraction peak intensity of AgCl (200) crystal plane at 32.3° decreases after cycle experiment, implying that part of AgCl is decomposed during the photocatalytic experiment [43]. The positions of other peaks are unchanged; however, the peak intensity decreases slightly, which may be caused by a small amount of undegraded MB molecules covering the surface of Ag@AgCl-ARB [44,45]. Meanwhile, it also causes the decline in photocatalytic activity, which is consistent with the cycling experimental results.

Inductively coupled plasma optical emission spectrometer was used to investigate the silver ion leached out from the photocatalyst in the supernatant after reaction. It is measured to be $0.0660 \pm 0.0003 \, \text{mg/L}$ in the solution, indicating that a small amount of Ag ion was leached into the solution.

3.7 Photodegradation mechanism

Figure 10 shows the results of active group capture experiment of Ag@AgCl-ARB. After adding BQ, IPA, and AO in MB degradation system, the order of photocatalytic degradation degrees of MB in the samples are BQ (30.8%) < IPA (76.5%) < AO (84.2%) < no Scavenger (97.3%), which suggests that O_2^- is the main active species, while O_2^+ of the secondary active species.

The formation of O_2^- was further verified by the nitro blue tetrazole (NBT) experiment. Figure 11(a) shows the absorbance curves of Ag@AgCl-ARB. With the increase in illumination time, the absorbance of NBT decreases gradually, which verifies the formation of O_2^- species [46–48]. Figure 11(b) shows the NBT absorbance curves of ARB and Ag@AgCl-ARB after 30 min irradiation. The NBT absorbance of Ag@AgCl-ARB is lower than that of ARB, indicating that more O_2^- species are generated in Ag@AgCl-ARB photocatalyst compared to ARB, which is consistent with the PL spectra.

The band potential can be estimated through the electronegativity equation of $E_{\rm CB} = X - E_0 - E_{\rm g}/2$ and $E_{\rm VB} = E_{\rm g} + E_{\rm CB}$, where $E_{\rm VB}$ is the valence band potential, $E_{\rm CB}$ is the conduction band potential, E_0 is the free electron energy on the hydrogen scale ($E_0 = 4.5 \, {\rm eV}$), $E_{\rm g}$ is the bandgap energy of the photocatalytic material, and X is the absolute electronegativity of the semiconductor [49–51]. Based on the DRS result (the band gap of

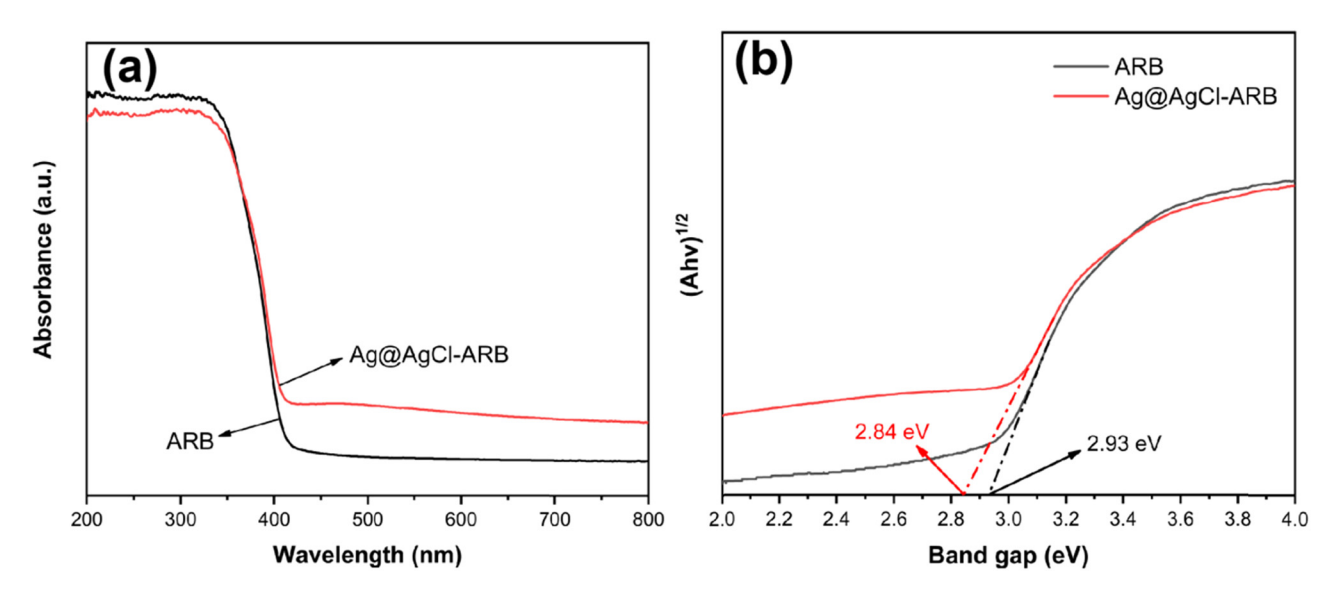


Figure 6: UV-visible absorption spectra (a) and band gap (b) of the samples.

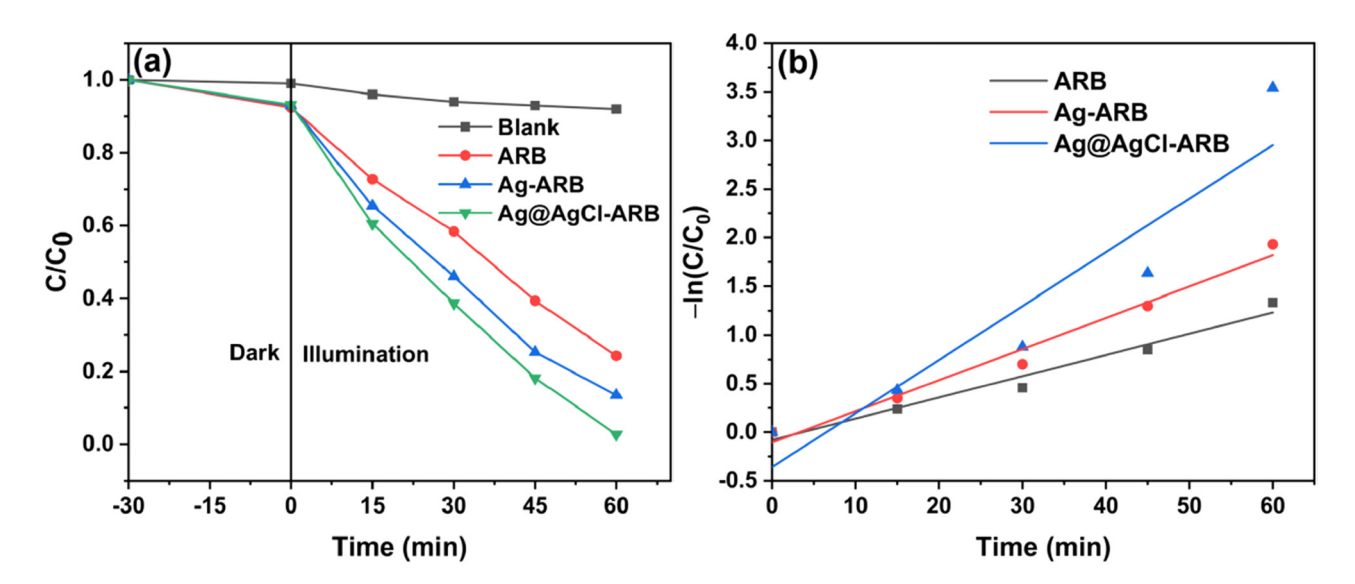


Figure 7: Degradation degree curves (a) and kinetic curves (b) of ARB, Ag-ARB, and Ag@AgCl-ARB.

ARB = 2.93 eV), the E_{CB} and E_{VB} of ARB are -0.15 and 2.78 eV, respectively. ARB consists of anatase, rutile, and brookite, and brookite shows the highest conduction band, followed by anatase and rutile [20,44,52,53]. On the other hand, the E_{CB} and E_{VB} of AgCl are determined to be -0.06 and 3.2 eV [54]. Based on the above content, a possible mechanism of the photogenerated charges separation and transfer for Ag@AgCl-ARB is proposed, as shown in Figure 12. In UV light region, photogenerated charges are generated, as TiO2 is three phase mixed crystal structure, which can accelerate the migration of carriers [52,53]. Moreover, the conduction bands of TiO₂ and AgCl are higher than the Fermi level of metallic Ag, and the photogenerated electrons generated in TiO₂ and AgCl will transfer to Ag particles, further inhibiting the recombination [54–57]. In visible light region, due to the SPR effect of Ag, the hot-electrons generated in Ag particles can be transferred to the conduction band of TiO2 and AgCl, which are captured by O2 to generate $\cdot O_2^-$ radicals, advancing the photocatalytic activity [58]. On the other hand, the holes will oxidize Cl⁻ to form Cl⁰ radicals, which also contributes to the

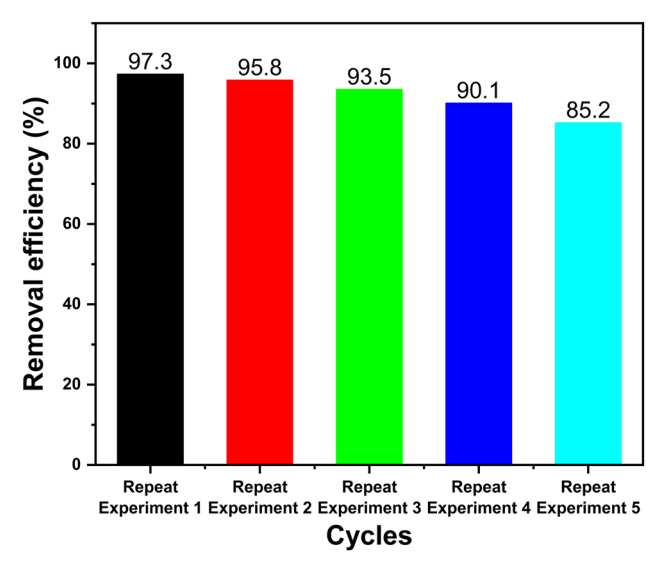


Figure 8: The reuse experiment of Ag@AgCl-ARB photocatalyst for MB degradation.

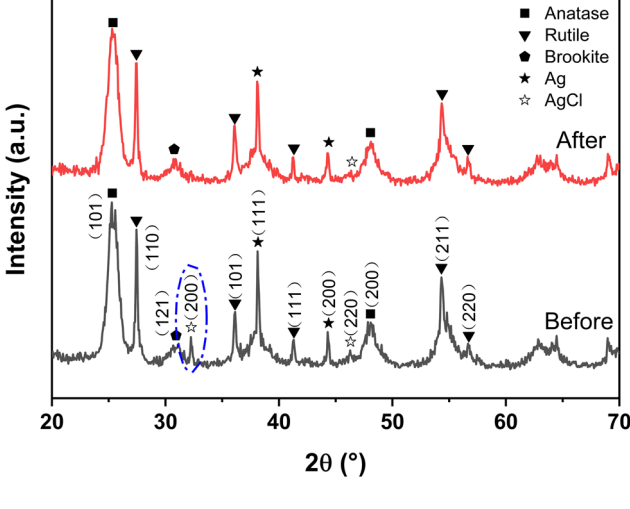


Figure 9: XRD patterns of Ag@AgCl-ARB photocatalyst before and after the photocatalytic experiment.

improvement in the photocatalytic activity [18,59]. Consequently, Ag@AgCl-ARB exhibits the best photocatalytic performance.

4 Conclusion

ARB and Ag@AgCl-ARB were prepared by one step hydrothermal method. ARB shows a three-phase mixed crystal structure composed of anatase, rutile, and brookite. Ag@AgCl modification does not change the crystal structure of ARB. The formation of Ag@AgCl-ARB heterojunctions is advantageous to the separation of photogenerated charges and the absorption of visible light,

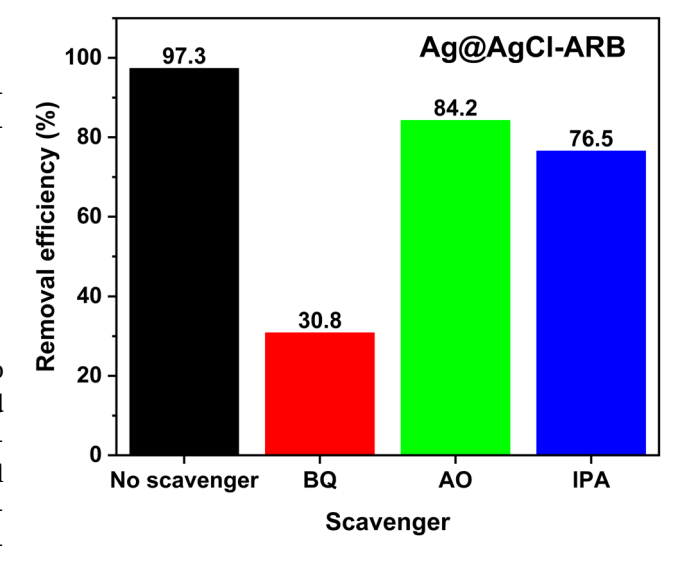


Figure 10: Active species experiment of Ag@AgCl-ARB.

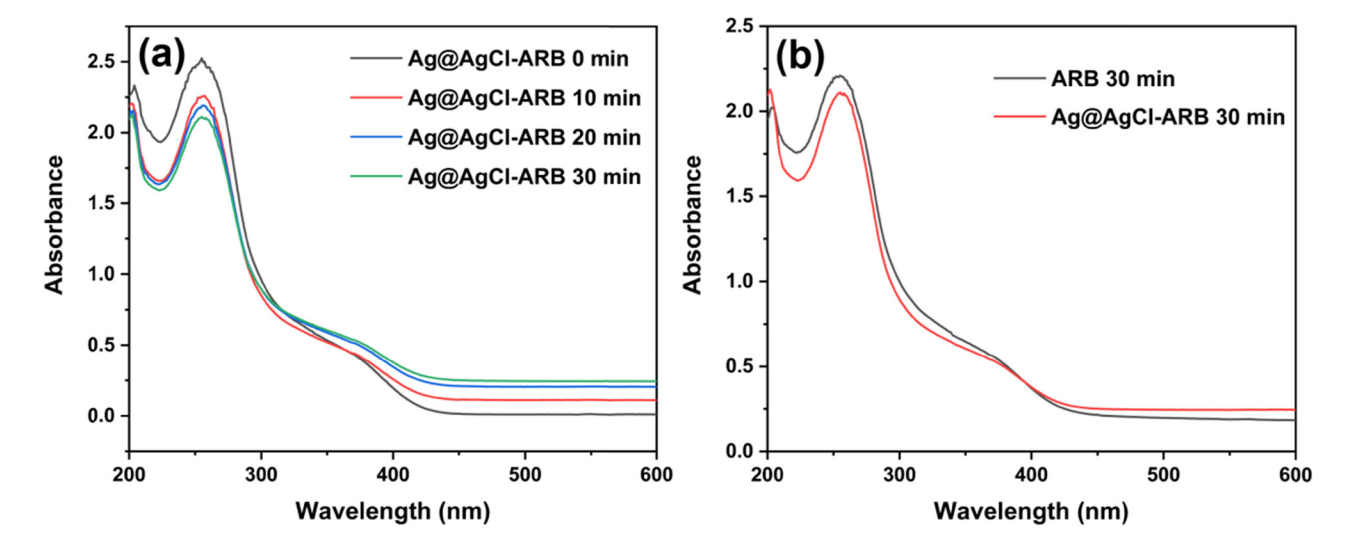


Figure 11: The NBT absorbance curves of Ag@AgCl-ARB with increasing time (a) and the comparison of ARB and Ag@AgCl-ARB (b).

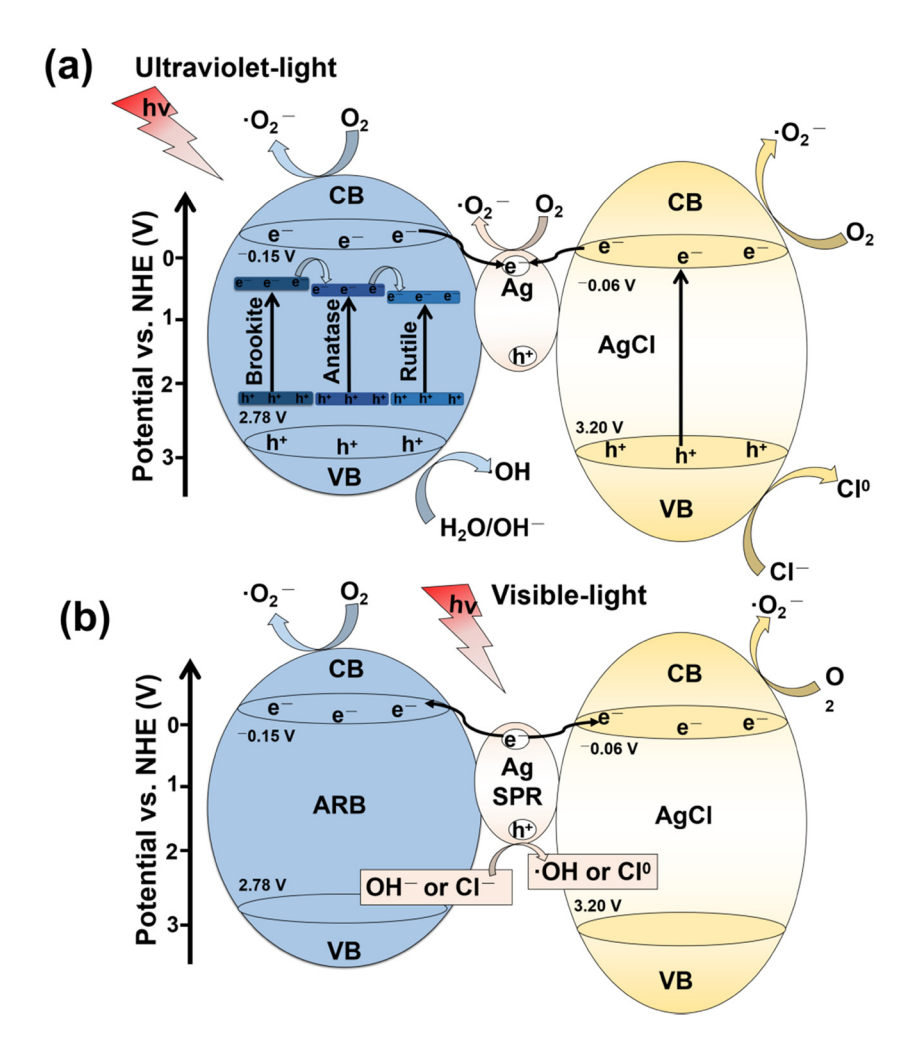


Figure 12: Schematic illustration of the charge separation and transfer in the Ag@AgCl-ARB photocatalysts under ultraviolet light (a) and visible light irradiation (b).

which can be explained by the fact that Ag@AgCl-ARB exhibits the highest photocatalytic activity.

Funding information: This study was supported by the Higher Education Talent Quality and Teaching Reform Project of Sichuan Province (JG2021-1104), the Talent Training Quality and Teaching Reform Project of Chengdu University (cdjgb2022033), and the Key Research and Development Projects of Liangshan Prefecture Science and Technology Bureau of Sichuan Province (21ZDYF0202).

Author contributions: All authors have accepted responsibility for the entire content of this manuscript and approved its submission.

Conflict of interest: The authors state no conflict of interest.

References

- [1] Mahmoodi NM, Taghizadeh M, Taghizadeh A. Activated carbon/metal-organic framework composite as a bio-based novel green adsorbent: preparation and mathematical pollutant removal modeling. J Mol Liq. 2019;277:310–22.
- [2] Mahmoodi NM. Dendrimer functionalized nanoarchitecture: synthesis and binary system dye removal. J Taiwan Inst Chem E. 2014;45(4):2008–20.
- [3] Mahmoodi NM. Manganese ferrite nanoparticle: synthesis, characterization, and photocatalytic dye degradation ability. Desalin Water Treat. 2015;53(1):84–90.
- [4] Yu XJ, Zhang J, Zhang J, Niu JF, Zhao J, Wei YC, et al. Photocatalytic degradation of ciprofloxacin using Zn-doped Cu₂O particles: analysis of degradation pathways and intermediates. Chem Eng J. 2019;374:316–27.
- [5] Li FH, Kang YP, Chen M, Liu GG, Lv WY, Yao K, et al. Photocatalytic degradation and removal mechanism of ibuprofen via monoclinic BiVO₄ under simulated solar light. Chemosphere. 2016;150:139-44.

- Mahmoodi NM, Limaee NY, Arami M, Borhany S, Mohammad-Taheri M. Nanophotocatalysis using nanoparticles of titania mineralization and finite element modelling of solophenyl dye decolorization. J Photoch Photobio A. 2007;189:1-6.
- Li M, Zhang JY, Zhang Y. First-principles calculation of compensated (2N, W) codoping impacts on band gap engineering in anatase TiO2. Chem Phys Lett. 2012;527:63-6.
- [8] Chen Y, Xiang ZY, Wang DS, Kang J, Qi HS. Effective photocatalytic degradation and physical adsorption of methylene blue using cellulose/GO/TiO2 hydrogels. RSC Adv. 2020;10:23936-43.
- [9] Lin XX, Rong F, Fu DG, Yuan CW. Enhanced photocatalytic activity of fluorine doped TiO2 loaded with Ag for degradation of organic pollutants. Powder Technol. 2012:219:173-8.
- [10] Bousiakou LG, Dobson PJ, Jurkin T, Marić I, Aldossary O, Ivanda M. Optical, structural and semiconducting properties of Mn doped TiO₂ nanoparticles for cosmetic applications. J King Saud Univ Sci. 2022;34:101818.
- [11] Asahi R, Taga Y, Mannstadt W, Freeman AJ. Electronic and optical properties of anatase TiO2. Phys Rev B. 2000;61(11):7459-65.
- [12] Serga V, Burve R, Krumina A, Romanova M, Kotomin EA, Popov AI. Extraction-pyrolytic method for TiO2 polymorphs production. Crystals. 2021;11:431.
- [13] Ziarati A, Badiei A, Luque R. Black hollow TiO₂ nanocubes: Advanced nanoarchitectures for efficient visible light photocatalytic applications. Appl Catal B-Environ. 2018;238:177-83.
- [14] Hou CT, Liu HY, Bakhtari MF. Preparation of Ag SPR-promoted TiO₂-{001}/HTiOF₃ photocatalyst with oxygen vacancies for highly efficient degradation of tetracycline hydrochloride. Mat Sci Semicon Proc. 2021;136:106142.
- [15] Hu HH, Qian DG, Lin P, Ding ZX, Cui C. Oxygen vacancies mediated in-situ growth of noble-metal (Ag, Au, Pt) nanoparticles on 3D TiO₂ hierarchical spheres for efficient photocatalytic hydrogen evolution from water splitting. ScienceDirect. 2020:45:629-39.
- [16] Zhu XD, Liu H, Wang J, Dai HL, Bai Y, Feng W, et al. Investigation of photocatalytic activity of Ag-rutile heterojunctions. Micro Nano Lett. 2020;15(15):1130-3.
- [17] Xu XY, Wu CB, Guo AY, Qin BP, Sun YF, Zhao CM, et al. Visiblelight photocatalysis of organic contaminants and disinfection using biomimetic-synthesized TiO₂-Ag-AgCl composite. Appl Surf Sci. 2022;588:152886.
- [18] Wang YF, Zhang M, Li J, Yang HC, Gao J, He G, et al. Construction of Ag@AgCl decorated TiO2 nanorod array film with optimized photoelectrochemical and photocatalytic performance. Appl Surf Sci. 2019;476:84-93.
- [19] Azizi-Toupkanloo H, Karimi-Nazarabad M, Amini GR, Darroudi A. Immobilization of AgCl@TiO2 on the woven wire mesh: sunlight-responsive environmental photocatalyst with high durability. Sol Energy. 2020;196:653-62.
- [20] Zhu XD, Zhou Q, Xia YW, Wang J, Chen HJ, Xu Q, et al. Preparation and characterization of Cu-doped TiO2 nanomaterials with anatase/rutile/brookite triphasic structure and their photocatalytic activity. J Mater Sci-Mater El. 2021;32(16):21511-24.
- [21] Preethi LK, Mathews T, Nand M, Jha SN, Gopinath CS, Dash S. Band alignment and charge transfer pathway in three phase anatase-rutile-brookite TiO2 nanotubes: an efficient photocatalyst for water splitting. Appl Catal B-Environ. 2017;218:9-19.

- [22] Mutuma BK, Shao GN, Kim WD, Kim HT. Sol-gel synthesis of mesoporous anatase-brookite and anatase-brookite-rutile TiO₂ nanoparticles and their photocatalytic properties. J Colloid Interf Sci. 2015;442:1-7.
- [23] Zhou GB, Jiang L, Dong YL, Li R, He DP. Engineering the exposed facets and open-coordinated sites of brookite TiO2 to boost the loaded Ru nanoparticle efficiency in benzene selective hydrogenation. Appl Surf Sci. 2019;486:187-97.
- [24] Ding MZ, Miao XL, Cao LJ, Zhang CM, Ping YX. Core-shell nanostructured SiO2@a-TiO2@Ag composite with high capacity and safety for Li-ion battery anode. Mater Lett. 2022;308:131276.
- [25] Padmini M, Balaganapathi T, Thilakan P. Mesoporous rutile TiO₂: synthesis, characterization and photocatalytic performance studies. Mater Res Bull. 2021;144:111480.
- [26] Granbohm H, Kulmala K, Iyer A, Ge YL, Hannula S-P. Preparation and photocatalytic activity of quaternary GO/TiO2/Ag/AgCl nanocomposites. Water Air Soil Poll. 2017;228(4):1-16.
- [27] Sun Y, Gao Y, Zhao BS, Xu S, Luo CH, Zhao Q. One-step hydrothermal preparation and characterization of ZnO-TiO₂ nanocomposites for photocatalytic activity. Mater Res Exp. 2020;7:085010.
- [28] Zhang Y, Wang T, Zhou M, Wang Y, Zhang ZM. Hydrothermal preparation of Ag-TiO₂ nanostructures with exposed {001}/ {101} facets for enhancing visible light photocatalytic activity. Ceram Int. 2017;43:3118-26.
- [29] Lu LY, Wang GH, Xiong ZW, Hu ZF, Liao YW, Wang J, et al. Enhanced photocatalytic activity under visible light by the synergistic effects of plasmonics and Ti3+ -doping at the Ag/TiO_{2-x} heterojunction. Ceram Int. 2020;46:10667-77.
- [30] Yin HY, Wang XL, Wang L, Nie QL, Zhang Y, Yuan QL, et al. Ag/AgCl modified self-doped TiO₂ hollow sphere with enhanced visible light photocatalytic activity. J Alloy Compd. 2016;657:44-52.
- [31] Liu SM, Zhu DL, Zhu JL, Yang Q, Wu HJ. Preparation of Ag@AgCl-doped TiO2/sepiolite and its photocatalytic mechanism under visible light. J Env Sci. 2017;60:43-52.
- [32] Zhu LD, Opulencia MJC, Bokov DO, Krasnyuk II, Su CH, Nguyen HC, et al. Synthesis of Ag-coated on a wrinkled SiO2@TiO2 architectural photocatalyst: new method of wrinkled shell for use of semiconductors in the visible light range and penicillin antibiotic degradation. Alex Eng J. 2022;61:9315-34.
- [33] Ali T, Ahmed A, Alam U, Uddin I, Tripathi P, Muneer M. Enhanced photocatalytic and antibacterial activities of Ag-doped TiO₂ nanoparticles under visible light. Mater Chem Phys. 2018;212:325-35.
- [34] Zheng S, Li XJ, Zhang JY, Wang JF, Zhao CR, Hu X, et al. Onestep preparation of MoO_x/ZnS/ZnO composite and its excellent performance in piezocatalytic degradation of rhodamine B under ultrasonic vibration. J Env Sci. 2023;125:1-13.
- [35] Feng Z, Zeng L, Zhang QL, Ge SF, Zhao XY, Lin HJ, et al. In situ preparation of $g-C_3N_4/Bi_4O_5I_2$ complex and its elevated photoactivity in methyl orange degradation under visible light. J Env Sci. 2020;87:149-62.
- [36] Chen PF, Chen L, Ge SF, Zhang WQ, Wu MF, Xing PX, et al. Microwave heating preparation of phosphorus doped g-C₃N₄ and its enhanced performance for photocatalytic H₂ evolution in the help of Ag₃PO₄ nanoparticles. Int J Hydrog Energ. 2020;45:14354-67.

- [37] Zeng L, Zhe F, Wang Y, Zhang QL, Zhao XY, Hu X, et al. Preparation of interstitial carbon doped BiOI for enhanced performance in photocatalytic nitrogen fixation and methyl orange degradation. J Colloid Interf Sci. 2019;539:563–74.
- [38] Haryński L, Olejnik A, Grochowska K, Siuzdak K. A facile method for Tauc exponent and corresponding electronic transitions determination in semiconductors directly from UV-Vis spectroscopy data. Opt Mater. 2022;127:112205.
- [39] Soumya S, Joe IH. A combined experimental and quantum chemical study on molecular structure, spectroscopic properties and biological activity of anti-inflammatory glucocorticosteroid drug, dexamethasone. J Mol Struct. 2021;1245:130999.
- [40] Shkir M, Khan ZR, Khan A, Chandekar KV, Sayed MA, AlFaify S. A comprehensive study on structure, opto-nonlinear and photoluminescence properties of Co₃O₄ nanostructured thin films: An effect of Gd doping concentrations. Ceram Int. 2022;48:14550–59.
- [41] Xu WC, Lai SF, Pillai SC, Chu W, Hu Y, Jiang XD, et al. Visible light photocatalytic degradation of tetracycline with porous Ag/graphite carbon nitride plasmonic composite: degradation pathways and mechanism. J Colloid Interf Sci. 2020;574:110-21.
- [42] Oveisi M, Mahmoodi NM, Asli MA. Facile and green synthesis of metal-organic framework/inorganic nanofiber using electrospinning for recyclable visible-light photocatalysis. J Clean Prod. 2019;222:669–84.
- [43] Prakash K, Kumar PS, Pandiaraj S, Saravanakumar K, Karuthapandian S. Controllable synthesis of SnO₂ photocatalyst with superior photocatalytic activity for the degradation of methylene blue dye solution. J Exp Nanosci. 2016;11(14):1138-55.
- [44] Tang M, Xia YW, Yang DX, Lu SJ, Zhu XD, Tang RY, et al. Ag decoration and SnO₂ coupling modified anatase/rutile mixed crystal TiO₂ composite photocatalyst for enhancement of photocatalytic degradation towards tetracycline hydrochloride. Nanomaterials. 2022;12:873.
- [45] Wang Y, Qiao MZ, Lv J, Xu GQ, Zheng ZX, Zhang XY, et al. $g-C_3N_4/g-C_3N_4$ isotype heterojunction as an efficient platform for direct photodegradation of antibiotic. Fuller Nanotub Car N. 2018;26(4):210–7.
- [46] Zhu XD, Wang J, Yang DX, Liu JW, He LL, Tang M, et al. Fabrication, characterization and high photocatalytic activity of Ag-ZnO heterojunctions under UV-visible light. RSC Adv. 2021;11:27257-66.
- [47] Li J, Wan YJ, Li YJ, Yao G, Lai B. Surface Fe(III)/Fe(II) cycle promoted the degradation of atrazine by peroxymonosulfate activation in the presence of hydroxylamine. Appl Catal B-Environ. 2019;256:117782.

- [48] Qin JX, Wang J, Yang JJ, Hu Y, Fu ML, Ye DQ. Metal organic framework derivative-TiO₂ composite as efficient and durable photocatalyst for the degradation of toluene. Appl Catal B-Environ. 2020;267:118667.
- [49] Ren FZ, Zhang JH, Wang YX. Enhanced photocatalytic activities of Bi₂WO₆ by introducing Zn to replace Bi lattice sites: A firstprinciples study. RSC Adv. 2015;5:29058-65.
- [50] Wen XJ, Niu CG, Ruan M, Zhang L, Zeng GM. Agl nanoparticlesdecorated CeO₂ microsheets photocatalyst for the degradation of organic dye and tetracycline under visible-light irradiation. J Colloid Interf Sci. 2017;497:368-77.
- [51] Alhaddad M, Ismail AA, Alghamdi YG, Al-Khathami ND, Mohamed RM. Co₃O₄ nanoparticles accommodated mesoporous TiO₂ framework as an excellent photocatalyst with enhanced photocatalytic properties. Opt Mater. 2022;131:112643.
- [52] Wang HL, Gao XY, Duan GR, Yang XJ, Liu XH. Facile preparation of anatase-brookite-rutile mixed-phase N-doped TiO₂ with high visible-light photocatalytic activity. J Env Chem Eng. 2015;3:603–8.
- [53] Benjwal P, De B, Kar KK. 1-D and 2-D morphology of metal cation co-doped (Zn, Mn) TiO₂ and investigation of their photocatalytic activity. Appl Surf Sci. 2018;427:262-72.
- [54] Yang QL, Hu MY, Guo J, Ge ZH, Feng J. Synthesis and enhanced photocatalytic performance of Ag/AgCl/TiO₂ nanocomposites prepared by ion exchange method. J Materiomics. 2018;4:402-11.
- [55] Xue XL, Gong XW, Chen XY, Chen BY. A facile synthesis of Ag/Ag₂O@TiO₂ for toluene degradation under UV-visible light: Effect of Ag formation by partial reduction of Ag₂O on photocatalyst stability. J Phys Chem Solids. 2021;150:109799.
- [56] Chen L, Zhang WQ, Wang JF, Li XJ, Li Y, Hu X, et al. High piezo/photocatalytic efficiency of Ag/Bi₅O₇I nanocomposite using mechanical and solar energy for N₂ fixation and methyl orange degradation. Green Energy Env. 2021. doi: 10.1016/j.gee.2021.04.009.
- [57] Li ZY, Zhang QL, Wang LK, Yang JY, Wu Y, He YM. Novel application of Ag/PbBiO₂I nanocomposite in piezocatalytic degradation of rhodamine B via harvesting ultrasonic vibration energy. Ultrason Sonochem. 2021;78:105729.
- [58] Zhang GH, Wang JC, Zhang HR, Zhang TY, Jiang S, Li B, et al. Facile synthesize hierarchical tubular micro-nano structured AgCl/Ag/TiO₂ hybrid with favorable visible light photocatalytic performance. J Alloy Compd. 2021;855(2):157512.
- [59] Mahmoodi NM, Taghizadeh A, Taghizadeh M, Abdi J. In situ deposition of Ag/AgCl on the surface of magnetic metalorganic framework nanocomposite and its application for the visible-light photocatalytic degradation of Rhodamine dye. J Hazard Mater. 2019;378:120741.